References and Notes

1. A. Dodabalapur *et al.*, *Appl. Phys. Lett.* **73**, 142 (1998).
2. H. Sirringhaus, N. Tessler, R. H. Friend, *Science* **280**, 1741 (1998).
3. R. J. Curry, W. P. Gillin, *Appl. Phys. Lett.* **75**, 1380 (1999).
4. L. H. Slooff *et al.*, *Appl. Phys. Lett.* **78**, 2122 (2001).
5. Y. Kawamura, Y. Wada, M. Iwamuro, T. Kitamura, S. Yanagida, *Chem. Lett.* **2000**, 280 (2000).
6. L. H. Slooff *et al.*, *J. Appl. Phys.* **83**, 497 (1998).
7. R. J. Curry, W. P. Gillin, A. P. Knights, R. Gwilliam, *Opt. Mater.* **17**, 161 (2001).
8. E. Desurvire, *Erbium Doped Fiber Amplifiers: Principles and Applications* (Wiley, New York, 1994).
9. A. D. Yoffe, *Adv. Phys.* **50**, 1 (2001).
10. V. L. Colvin, M. C. Schlamp, A. P. Alivisatos, *Nature* **370**, 354 (1994).
11. B. O. Dabbousi, M. G. Bawendi, O. Onitsuka, M. F. Rubner, *Appl. Phys. Lett.* **66**, 1316 (1995).
12. M. C. Schlamp, X. G. Peng, A. P. Alivisatos, *J. Appl. Phys.* **82**, 5837 (1997).
13. H. Mattoussi *et al.*, *J. Appl. Phys.* **83**, 7965 (1998).
14. N. C. Greenham, X. G. Peng, A. P. Alivisatos, *Phys. Rev. B* **54**, 17628 (1996).
15. Y. W. Cao, U. Banin, *Angew. Chem. Int. Ed. Engl.* **38**, 3692 (1999).
16. ———, *J. Am. Chem. Soc.* **122**, 9692 (2000).
17. M. A. Baldo, M. E. Thompson, S. R. Forrest, *Nature* **403**, 750 (2000).
18. ADSDYES, www.adsdyes.com (American Dye Source Inc.).
19. The conversion from external to internal efficiency in subwavelength devices depends on many device parameters (*20*), and hence we can only estimate a range for the internal efficiency of 1.5 to 3%.
20. N. Tessler, *Appl. Phys. Lett.* **77**, 1897 (2000).
21. ———, in *Elsevier Encyclopedia of Materials: Science and Technology*, E. J. Kramer, G. Hadziioannou, Eds. (Elsevier, New York, 2001), pp. 4402–4408.
22. The conjugated polymer hosts were used as purchased (MEH-PPV or ADS100RE and F6BT or ADS133) without any additional chemical treatment.
23. Glass or indium tin oxide (ITO)–glass substrates were used for optical and electrical measurements, respectively. The nanocomposite solution was prepared by first preparing NC and polymer solutions in toluene having weight concentrations of ~50 mg/ml and 5 mg/ml, respectively. The LED preparation procedure was as follows: The ITO-glass substrate was plasma-cleaned and then covered by PEDOT (Bayer Baytron P TP Al), which was then annealed at 110°C for 30 min. After substrate cooling, the nanocomposite solution (~1:1 volume ratio) was spin-coated on the ITO-PEDOT substrate with a resulting thickness of ~100 nm. This structure was then annealed at 90°C for 30 min and allowed to slowly cool down under dry vacuum. Finally, Ca-Al contacts were evaporated at working pressure within the low (10^{-7} mbar) range. Pixel area was 1 mm by 1 mm. All steps, including optical and electrical characterization of the LEDs, were carried out within an inert glove box system having sub-ppm levels of water and oxygen.
24. N. C. Greenham, R. H. Friend, D. D. C. Bradley, *Adv. Mater.* **6**, 491 (1994).
25. G. G. Malliaras, J. C. Scott, *J. Appl. Phys.* **83**, 5399 (1998).
26. K. C. Kao, W. Hwang, *Electrical Transport in Solids*, vol. 14 of *International Series in the Science of the Solid State* (Pergamon, New York, 1981).

27. We thank R. Beadle for his help with the experimental setup. Supported in part by Israel Science Foundation grants 99/00-12.5 (U.B.) and 56/00-11.6 (N.T.).

19 November 2001; accepted 17 January 2002

Otolith $\delta^{18}O$ Record of Mid-Holocene Sea Surface Temperatures in Peru

C. Fred T. Andrus,[1]* Douglas E. Crowe,[1] Daniel H. Sandweiss,[2] Elizabeth J. Reitz,[3] Christopher S. Romanek[1,4]

Peruvian sea catfish (*Galeichthys peruvianus*) sagittal otoliths preserve a record of modern and mid-Holocene sea surface temperatures (SSTs). Oxygen isotope profiles in otoliths excavated from Ostra [6010 ± 90 years before the present (yr B.P.); 8°55′S] indicate that summer SSTs were ~3°C warmer than those of the present. Siches otoliths (6450 ± 110 yr B.P.; 4°40′S) recorded mean annual temperatures ~3° to 4°C warmer than were measured under modern conditions. Trophic level and population diversity and equitability data from these faunal assemblages and other Peruvian archaeological sites support the isotope interpretations and suggest that upwelling of the Peru-Chile current intensified after ~5000 yr B.P.

Evidence that modern El Niño–Southern Oscillation (ENSO) conditions (e.g., Pacific SSTs, precipitation, and frequency of El Niño warm events) began after the mid-Holocene is increasing. Ecuadorian lake sediments record lower frequency ENSO before 5000 yr B.P. (*1*, *2*). Western Pacific coral oxygen isotope ($\delta^{18}O$) and Sr/Ca data document warmer western Pacific SSTs, increased evaporation ~5350 yr B.P. (*3*), and decreased ENSO ~6500 yr B.P. (*4*). Western Pacific terrestrial pollen records suggest that ENSO was less active before ~4000 yr B.P. (*5*). Ice cores from Huascarán, Peru, indicate that the local climate was warmer than the modern climate from 8400 to 5200 yr B.P. (*6*). Thermally anomalous molluscan assemblages (TAMAs) and tropical fish in Peruvian middens north of 10°S suggest that there were warmer SSTs in the eastern Pacific from ~8000 to 5000 yr B.P. (*7*, *8*). Model results for 6 and 11 thousand years ago suggest a slightly warmer annual mean SST along the coast of Ecuador and northern Peru than at present (*9*).

In contrast, some ENSO climate models incorporating seasonality changes caused by perihelion timing indicate a cool eastern Pacific before 5000 yr B.P. (*10*, *11*). Field evidence of a cool mid-Holocene eastern Pacific includes Peruvian coastal geomorphology and soils that suggest persistent aridity (*12*, *13*). Advocates of this position argue that TAMAs (*7*, *8*) resulted from restricted warm-water embayments protecting species that would otherwise not survive in the cool open ocean (*8*, *12*, *14*).

The lack of quantitative seasonal SST data from mid-Holocene northern coastal Peru makes it difficult to resolve these different interpretations (*7*, *11*). Our otolith data provide SST reconstructions that indicate that the eastern Pacific at ~6000 yr B.P. was seasonally warmer than today along the central coast of Peru and warmer year-round along the northern coast of Peru.

Otoliths are aragonite ($CaCO_3$) structures in fish used for acoustic perception and balance. They grow incrementally from the endolymph in alternating opaque and translucent bands that reflect biological and environmental growth conditions (*15*). Previous studies show that otolith aragonite precipitates in oxygen isotope equilibrium with seawater (*16*). The exchange reaction is temperature dependent; thus, the $\delta^{18}O$ composition of the otolith can be used as a temperature proxy (*16*, *17*).

The archaeological sites of Ostra (6250 ± 250 to 5160 ± 60 yr B.P.) and Siches (6590 ± 90 to 4930 ± 80 yr B.P.) are central to interpretations of warm eastern Pacific SSTs from 8000 to 5000 yr B.P. (*7*, *8*). Ostra is currently in a warm-temperate area, and Siches is transitional between the warm-tropical Panamanian and the cooler warm-temperate Peru-Chile provinces (Fig. 1). Both sites contain well-preserved otolith assemblages of several species, including *Galeichthys peruvianus* (*7*, *18*).

G. peruvianus was selected for analysis because it does not migrate, even in response to seasonal or ENSO-related SST changes. Typically, Ariidae catfish remain in nearshore habitats (*19*). They have large otoliths containing biannual growth banding, thus making them amenable to microsampling (Fig. 2). Modern *G. peruvianus* were caught

[1]Department of Geology, University of Georgia, Athens, GA 30602–2501, USA. [2]Department of Anthropology and Institute for Quaternary Research, S. Stevens Hall, University of Maine, Orono, ME 04469, USA. [3]Department of Anthropology and Georgia Museum of Natural History, Natural History Building, University of Georgia, Athens, GA 30602–1882, USA. [4]Savannah River Ecology Laboratory, Drawer E, Aiken, SC 29802, USA.

*To whom correspondence should be addressed. E-mail: andrus@gly.uga.edu

near Pimentel (n = 3 fish; 6°50′S) in July 1997, and near Huanchaco (n = 7 fish; ~8°10′S) in July 1998 and 1999, during and after the strong 1997–1998 ENSO event (Fig. 1), thus documenting the wide temperature tolerance of the fish.

Otoliths were analyzed for $\delta^{18}O$ by infrared laser microprobe (*20*) and conventional methods (*21*) to test the fidelity of the otolith temperature proxy (*22*). Seasonal variations were recorded in all otoliths sampled at 6-month or higher resolution (*21*, *22*). The stacked record of modern otolith $\delta^{18}O$ ($\delta^{18}O_{otolith}$) values varies in good agreement with what would be expected from observed SSTs, and both the 1991–1992 and 1997–1998 El Niño warm events were recorded as significant negative excursions in the $\delta^{18}O \rightarrow \delta^{18}O_{otolith}$ profiles (Fig. 3A) (*23*). The influence of fresh water on the $\delta^{18}O \rightarrow \delta^{18}O_{otolith}$ profiles was minimal based on comparisons with modeled $\delta^{18}O_{otolith}$ values derived from SST records from Puerto Chicama (8°S), measured water $\delta^{18}O$ ($\delta^{18}O_{water}$), and the experimentally determined paleotemperature equation for aragonite (*22–24*). This is not surprising given the steep shore face and low stream discharge on this desert coast.

The same methods used in the analysis of modern otoliths were applied to otoliths excavated from archaeological sites. Seven otoliths from Ostra were analyzed at a temporal resolution of 4 to 6 months. Figure 3B shows a representative Ostra $\delta^{18}O_{otolith}$ record. The mean $\delta^{18}O$ of these otoliths is −0.5 per mil (‰) (1σ = 0.5), with a mean seasonal $\delta^{18}O$ range of 1.6‰ (1σ = 0.6).

Five otoliths from Siches were analyzed at the same temporal resolution. Figure 3C shows one representative Siches $\delta^{18}O_{otolith}$ record. The mean $\delta^{18}O$ of these otoliths is −1.6‰ (1σ = 0.1), with a mean seasonal $\delta^{18}O$ range of 1‰ (1σ = 0.2).

Figure 3D depicts averaged $\delta^{18}O \rightarrow \delta^{18}O_{otolith}$ seasonal oscillations from both sites as well as modern collections. Ostra $\delta^{18}O_{otolith}$ values are 0.5‰ lower than those of modern otoliths. A t test comparing modern and Ostra mean $\delta^{18}O \rightarrow \delta^{18}O_{otolith}$ values indicates that this difference is insignificant (P = 0.774, n = 17 otoliths). Seasonal $\delta^{18}O \rightarrow \delta^{18}O_{otolith}$ variation is ~0.6‰ greater in Ostra otoliths as compared to modern otoliths. A t test of average seasonal variability based on the mean difference between $\delta^{18}O$ values in adjacent biannual bands shows that this difference is marginally significant (P = 0.044, n = 17 otoliths). Differences in summer $\delta^{18}O \rightarrow \delta^{18}O_{otolith}$ values are significant (P = 0.013, n = 68 summer increments, 17 otoliths), with Ostra $\delta^{18}O \rightarrow \delta^{18}O_{otolith}$ values being more negative. Winter differences are insignificant (P = 0.385, n = 70 winter increments, 17 otoliths).

Siches $\delta^{18}O_{otolith} \rightarrow \delta^{18}O_{otolith}$ values are ~1‰ more negative than model $\delta^{18}O$ values (the 1989–1999 mean = −0.8‰, average seasonal range = 0.8‰) derived from Paita SST data (*22*). The significance of this change cannot be measured against modern otoliths collected farther south, but the range of mean $\delta^{18}O \rightarrow \delta^{18}O_{otolith}$ values (–1.7 to 2.2‰) is one-half of the difference between measured and modeled data, indicating that the otolith data are robust. The seasonal range of $\delta^{18}O \rightarrow \delta^{18}O_{otolith}$ in Siches otoliths is similar to that of modern values.

Considering other contemporaneous paleoclimate data (*2–7*), and the match between the observed and modeled $\delta^{18}O_{otolith}$ data, the most plausible explanation for the archaeological $\delta^{18}O_{otolith}$ values is warmer summer SSTs at Ostra and nearly tropical conditions near Siches in the early mid-Holocene.

Alternative explanations are less tenable. It is unlikely that freshwater influx produced the negative excursions in $\delta^{18}O_{otolith}$ values. *G. peruvianus* avoids freshwater rivers in Peru; and precipitation, even during large ENSO events, would not dilute open coastal waters enough to affect $\delta^{18}O_{water}$ values (*21*). Furthermore, for $\delta^{18}O_{water}$ variation to cause the measured $\delta^{18}O_{otolith}$ values, it would have to vary seasonally at Ostra while remaining consistently more negative at Siches as compared to modern con-

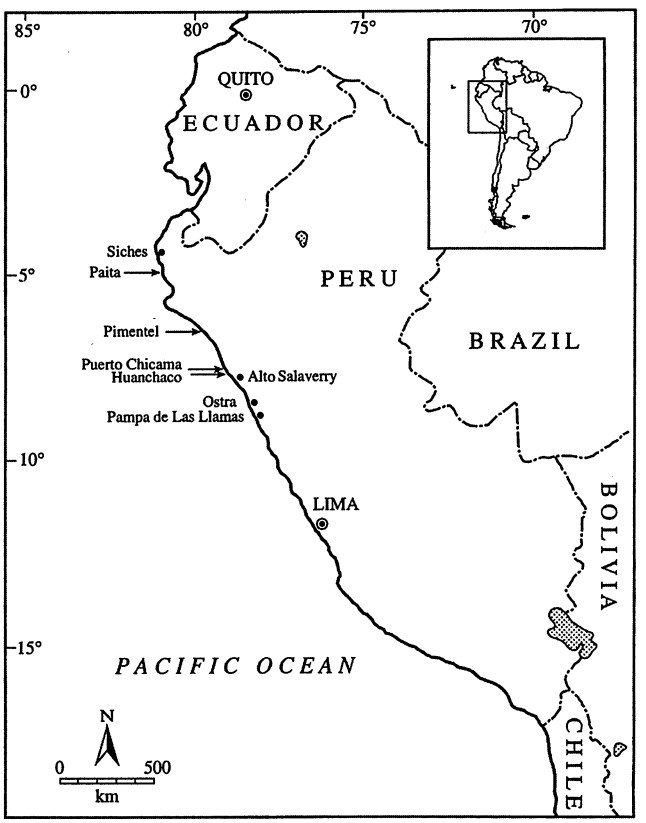

Fig. 1. Map of the research area showing archaeological sites, modern collection sites, and JISOA SST data stations mentioned in the text. The inset shows an outline of the study area.

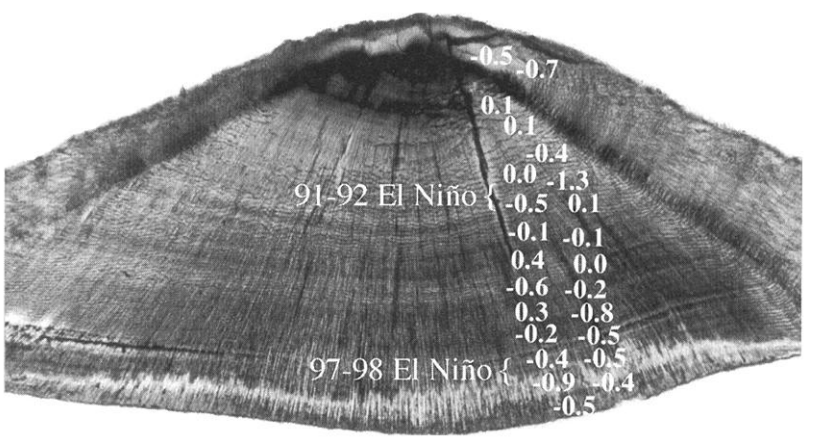

Fig. 2. Photomicrograph of a modern otolith in thin section. The field of view is ~1 cm. $\delta^{18}O$ values follow ontogeny.

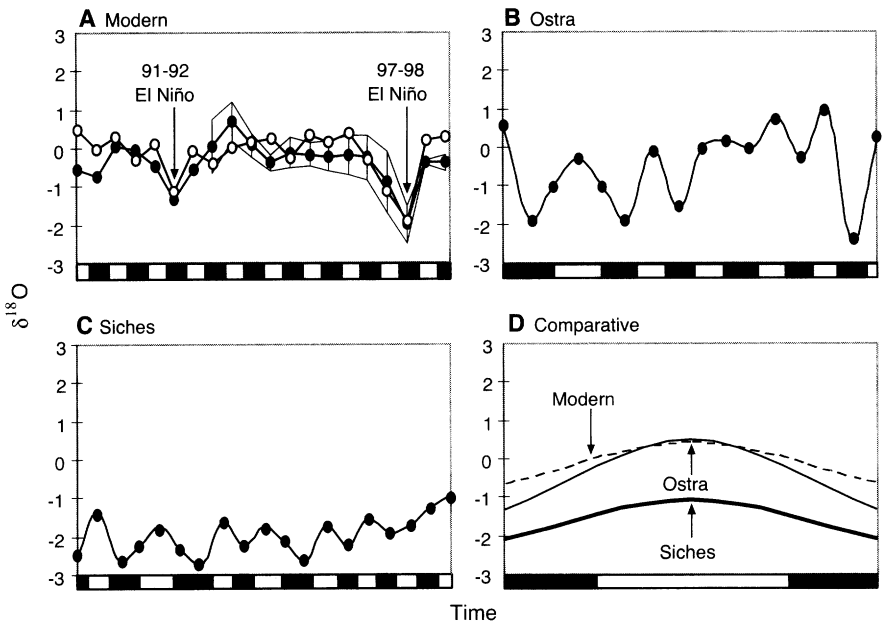

Fig. 3. *x* axes represent time from birth (left) to death (right). *y* axes are $\delta^{18}O$‰ relative to PDB. Horizontal bars at the bottom indicate the macroscopic increment type as seen in transmitted light. White, austral winter; black, austral summer. Precision limits are equal to the size of data points in (B) and (C). (**A**) Composite mean of 10 modern otoliths. The 1991–1992 and 1997–1998 El Niños are labeled with arrows. Solid circles represent $\delta^{18}O_{otolith}$; vertical lines represent 1σ from mean. Open circles represent $\delta^{18}O_{model}$. (**B**) Plot of one Ostra otolith; ~6 year record. (**C**) Plot of one Siches otolith; ~8 year record. (**D**) Seasonal $\delta^{18}O$ variation, based on mean values of light and dark bands, from modern otoliths (dashed line), Ostra otoliths (thin line), and Siches otoliths (thick line). A 1-year period beginning and ending in the austral summer is shown.

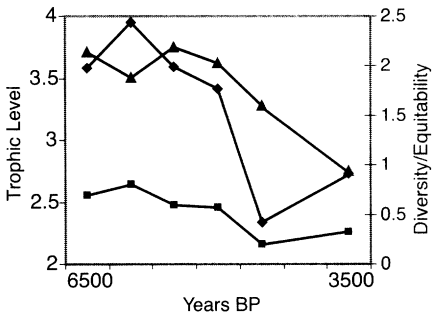

Fig. 4. Plot of mean trophic level, diversity, and equitability of vertebrate marine taxa at sites through time (*x* axis). At left, the *y* axis represents the trophic level (triangles). At right, the *y* axis represents the taxonomic diversity (diamonds) and equitability (squares). Sites, ranging from oldest to most recent, are as follows: Siches, Ostra, Siches–Lower Honda, Siches–Upper Honda, Alto Salaverry, and Pampa de Las Llamas-Moxeke.

ditions. Such systematic variation in $\delta^{18}O_{water}$ is unlikely. It is also unlikely that *G. peruvianus* behavior has changed since ~6000 yr B.P. to produce the observed $\delta^{18}O \rightarrow \delta^{18}O_{otolith}$ values at both sites. There is no evidence of ontogenetic migration in the modern or ancient isotope profiles, and modern fish of all size classes were caught in the same habitat. Thus, fish movement is unlikely to produce the observed variation in the archaeological otoliths.

However, these fish are not sessile, and their $\delta^{18}O \rightarrow \delta^{18}O_{otolith}$ profiles reflect a mean of the local waters in which they develop. The temperature record they preserve is not derived from a single potentially anomalous microclimate but reflects general coastal conditions in a region. Each otolith records the specific SST conditions under which the fish grew. As SST varies spatially even within the limited range of this fish, so do the $\delta^{18}O \rightarrow \delta^{18}O_{otolith}$ profiles among otoliths, but individual otolith SST histories from the same area can be combined to form an integrated regional temperature history.

The distribution of other taxa excavated from the Ostra and Siches sites supports the interpretation that the $\delta^{18}O_{otolith}$ values are a result of SST change. Ostra contains 60% warm-tropical and 40% warm-temperate vertebrate taxa [based on the minimum number of individuals (MNI)], and Siches contains 90% warm-tropical taxa (*7*, *18*). These distributions are consistent with pronounced seasonal SST variation at Ostra and a nearly tropical climate at Siches.

Warmer and more seasonal SSTs indicate diminished upwelling of the cool Peru-Chile current in northern Peru before 5000 yr B.P. This would alter the trophic structure of finfish populations, so that lower trophic level species would be proportionally less abundant in the early mid-Holocene than at present, and the diversity and equitability of the taxa would be diminished. To test this hypothesis, the MNI of vertebrate taxa from all occupation periods of Ostra and Siches (*18*) were compared to the taxa from post–5000 yr B.P. sites (*25–27*) of Alto Salaverry and Pampa de Las Llamas-Moxeke (Fig. 1). Mean taxonomic diversity (*28*), equitability (*29*), and trophic level (*30–32*) all decreased after 5000 yr B.P. (Fig. 4), as indicated by greater numbers of anchovies in the more recent sites. These observations are consistent with the picture obtained from the otolith data.

Others have interpreted TAMAs at Ostra to be the result of a partially or completely enclosed embayment that provided a warm microclimate adjacent to a cool Pacific, permitting warm-temperate and warm-tropical taxa to coexist (*12–14*). However, the warm-tropical and warm-temperate mollusk assemblages are not contemporaneous, as demonstrated by age dates (*8*, *33*). Positive $\delta^{18}O$ values in TAMAs from the former Ostra embayment may indicate evaporative conditions (*34*). Our otolith data show more negative values, indicating that they record oceanic conditions. Further, Siches is not near any former embayment or river, so geomorphic explanations do not apply to data from that site. Therefore, invertebrate and vertebrate faunal assemblages at Ostra and Siches, and other similar assemblages that persist in the archaeological record from ~8000 to 5000 yr B.P., north of 10°S latitude (*7*, *8*), are best explained by SST change recorded in otoliths excavated from these sites.

References and Notes

1. All otolith age dates are reported in uncalibrated radiocarbon years. All other dates are as reported in the cited publications.
2. D. T. Rodbell *et al.*, *Science* **283**, 516 (1999).
3. M. K. Gagan *et al.*, *Science* **279**, 1014 (1998).
4. A. W. Tudhope *et al.*, *Science* **291**, 1511 (2001).
5. J. Shulmeister, B. G. Lees, *Holocene* **5**, 10 (1995).
6. L. G. Thompson *et al.*, *Science* **269**, 46 (1995).
7. D. H. Sandweiss, J. B. Richardson III, E. J. Reitz, H. B. Rollins, K. A. Maasch, *Science* **273**, 1531 (1996).
8. _____, *Science* **276**, 966 (1997).
9. Z. Liu, J. Kutzbach, L. Wu, *Geophys. Res. Lett.* **27**, 2265 (2000).
10. A. C. Clement, R. Seager, M. A. Cane, *Paleoceanography* **15**, 731 (2000).
11. A. B. G. Bush, *Quat. Res.* **55**, 25 (2001).
12. L. E. Wells, J. S. Noller, *Science* **276**, 966 (1997).
13. _____, *Geoarchaeology* **14**, 755 (1999).
14. T. J. DeVries *et al.*, *Science* **276**, 965 (1997).
15. C. S. Romanek, R. W. Gauldie, *Comp. Biochem. Physiol.* **114A**, 71 (1996).
16. S. R. Thorrold, S. E. Campana, C. M. Jones, P. K. Swart, *Geochim. Cosmochim Acta* **61**, 2909 (1997).
17. L. C. Ivany, W. P. Patterson, K. C. Lohmann, *Nature* **407**, 887 (2000).
18. E. J. Reitz, *Int. J. Osteoarch.* **11**, 163 (2001).
19. R. Cooke, in *Exploración de Recursos Faunísticos en Sistemas Adaptivos Americanos*, J. L. Lamata, Ed. (Arquelogía Contemporánea, 4, Buenos Aires, Argentina, 1993), pp. 57–74.
20. C. F. T. Andrus, D. E. Crowe, *J. Arch. Sci.* **27**, 33 (2000).
21. _____, C. S. Romanek, *Paleoceanography*, in press. Temporal resolution averaged ~4 months in laser extraction and ~6 months in micromill extraction (laser pits were ~100 μm in diameter and ~100 μm deep; micromill transects were ~100 μm deep with the width variable, based on the diameter of the growth band). Temporal control was based on incre-

mental growth as described in (*21*). Resolution decreased with ontogeny because of diminished increment width with age. $\delta^{18}O \rightarrow \delta^{18}O_{otolith}$ ratios are reported relative to Pee Dee belemnite (PDB) standard, and water oxygen isotope ratios are reported relative to Standard Mean Ocean Water (SMOW) using conventional per mil (‰) notation. Precision of isotope analyses is as follows: conventional H_3PO_4 extraction (of aragonite) is ± 0.1‰ (1σ), laser ablation extraction (of aragonite) is ±0.2‰ (1σ), and CO_2 equilibration (of water) is ± 0.1‰ (1σ). Precision was calculated based on between- and within-run comparisons of working standards.

22. SST data from the Joint Institute for the Study of the Atmosphere and the Oceans database can be found online at http://tao.atmos.washington.edu/data_sets/for Puerto Chicama (8°S, 1989–1999) and Paita (5°S, 1989–1998), and measured $\delta^{18}O_{water}$ values (–0.5 ± 0.2‰ 1σ; n = 4) were applied to the aragonite $\delta^{18}O$ temperature equation (*24*) to build models of $\delta^{18}O_{otolith}$ profiles.
23. Figure 3A compares model $\delta^{18}O_{otolith}$ values to the composite mean $\delta^{18}O$ of 10 modern otoliths. The composite was constructed by calculating the mean $\delta^{18}O$ value of each increment in every otolith. These values were averaged with all other contemporaneous increments to produce the 6-month time-average composite. The mean $\delta^{18}O$ of the modern otoliths is –0.1‰ (1σ = 0.4), with a mean seasonal $\delta^{18}O$ range of 1‰ (1σ = 0.3). Modeled and measured isotope profiles were strongly correlated, thus documenting $\delta^{18}O_{otolith}$ records as valid proxies for SSTs.
24. E. L. Grossman, T. L. Ku, *Chem. Geol.* **59**, 59 (1986).
25. S. Pozorski, T. Pozorski, *Ann. Carnegie Mus.* **48**, 337 (1979).
26. ___ →, *J. Field Archaeol.* **13**, 381 (1986).
27. E. J. Reitz, unpublished data.
28. C. E. Shannon, W. Weaver, *The Mathematical Theory of Communication* (Univ. of Illinois Press, Urbana, IL, 1949).
29. S. H. Hurlbert, *Ecology* **52**, 577 (1971).
30. D. Pauly, V. Christensen, *Nature* **374**, 255 (1995).
31. R. Froese, D. Pauly, *Fishbase*, online at www.fishbase.org (2 March, 2001).
32. Diversity was calculated by $H' = \sum_{i=1}^{S} (p_i)(\log p_i)$, where H' = diversity, $\sum_{i=1}^{S}$ = the sum of all taxa, and p_i = relative abundance of i^{th} taxon (*28*). Equitability was calculated by $V' = H'/\log S$, where V' = equitability and S = number of taxa (*29*). Trophic level determination was based on data in (*31*), or the nearest approximation based on analog species. Trophic value was determined for each taxon identified and multiplied by its MNI, and then the total of all trophic values was divided by total-site MNI. All sites were excavated in a similar fashion, and we used fine mesh-screen recovery, thus minimizing recovery bias and ensuring representative samples.
33. D. H. Sandweiss, K. A. Maasch, D. F. Belknap, J. B. Richardson III, H. B. Rollins, *J. Coastal Res.* **14**, 367 (1998).
34. C. Perrier, C. Hillaire-Marcel, L. Ortlieb, *Geogr. Phys. Quat.* **48**, 23 (1994).
35. We thank B. McClain for assistance with isotopic analysis and M. Cornejo for field assistance. Funded in part by grants from the Geological Society of America (C.F.T.A.), Explorer's Club International (C.F.T.A.), NSF grant ATM-0082213 (D.E.C.), The Heinz Charitable Trust (D.H.S.), the University of Maine Faculty Research Fund (D.H.S.), and Department of Energy grant DE-FC09-96SR18546 (C.S.R.).

26 April 2001; accepted 14 January 2002

Abrupt Decrease in Tropical Pacific Sea Surface Salinity at End of Little Ice Age

Erica J. Hendy,[1]* Michael K. Gagan,[1] Chantal A. Alibert,[1] Malcolm T. McCulloch,[1] Janice M. Lough,[2] Peter J. Isdale[2]

A 420-year history of strontium/calcium, uranium/calcium, and oxygen isotope ratios in eight coral cores from the Great Barrier Reef, Australia, indicates that sea surface temperature and salinity were higher in the 18th century than in the 20th century. An abrupt freshening after 1870 occurred simultaneously throughout the southwestern Pacific, coinciding with cooling tropical temperatures. Higher salinities between 1565 and 1870 are best explained by a combination of advection and wind-induced evaporation resulting from a strong latitudinal temperature gradient and intensified circulation. The global Little Ice Age glacial expansion may have been driven, in part, by greater poleward transport of water vapor from the tropical Pacific.

The Little Ice Age (LIA) appears in most Northern Hemisphere paleoclimate reconstructions as multiple, century-scale periods of anomalously cold, dry conditions between the 15th and late 19th centuries (*1–4*). Glacial advances in both hemispheres (*1*) and enhanced polar atmospheric circulation (*5*) suggest that the LIA was a global-scale event. With the exception of the Quelccaya ice core record from equatorial Peru (*6*), however, the sparse reconstructions of the LIA available from the tropics and Southern Hemisphere fail to identify synchronous cold periods (*7, 8*). An alternative scenario is that cooling during the LIA was restricted to higher latitudes (*9, 10*). We examine the nature of the LIA in the tropical southwestern Pacific since 1565 using coral proxies to reconstruct sea surface temperature (SST) and salinity (SSS), the key indicators of climate change within the tropical ocean-atmosphere system.

We present 420-year records of three coral paleoclimate tracers, $\delta^{18}O$, Sr/Ca, and U/Ca, constructed from replicated measurements of eight cores from massive *Porites* sp. colonies (Fig. 1). The cores were collected at seven reefs, 12 to 120 km apart, from the central Great Barrier Reef (GBR), Australia [for details and site maps, see (*11*)]. The use of multiple cores allows us to test the fidelity of individual tracers over century time scales and to establish regional-scale proxy climate signals. Coral $\delta^{18}O$, the most frequently used coral climate proxy tool, reflects a combination of SST and the seawater $\delta^{18}O$ composition. The latter responds to changes in SSS caused by shifts in seawater $\delta^{18}O$ produced by evaporation and freshwater input. By using parallel measurements of the coral paleothermometers Sr/Ca and U/Ca to determine SST, we are able to separate SST variation from changes in seawater $\delta^{18}O$ (*12, 13*). This approach allows us to resolve both SST and SSS over the past four centuries.

Five-year bulk increments were sampled for equivalent periods across all eight cores after cross-dating with ultraviolet (UV) fluorescent bands; x-radiography was used to reveal annual density banding (*14*). Fine powder was milled from 2-mm square-section grooves along the center of the coral growth axis, homogenized, and subsampled for stable isotope and trace element analysis (*15*). Figure 1 shows the replicated measurements combined into a composite record, with the variability between corals shown as a 95% confidence envelope calculated for each pentannual interval (*16*). Individual $\delta^{18}O$ records reproduce not only the century-scale trends in the composite $\delta^{18}O$ reconstruction but also decadal variations of up to 0.26‰, capturing on average 72% of the shared $\delta^{18}O$ signal. Intercoral variability is greater between individual Sr/Ca and U/Ca records, which share on average 33% and 26%, respectively, of the common variance. When converted to temperature by applying accepted SST-slope calibrations (*17, 18*), the Sr/Ca record is better constrained than the U/Ca record (Sr/Ca, ±0.3°C; U/Ca, ±0.5°C). This intercoral Sr/Ca variability is equivalent to that found between high-resolution seasonal records from *Porites* colonies at sites close to those used here (*13, 17*). However, multiple Sr/Ca or U/Ca records are required to reconstruct decadal to century-scale SST signals, which in the GBR are one-tenth the size of seasonal variations.

The Sr/Ca and U/Ca composite records, converted to SST anomalies (SSTA), are verified against GISST2.2 (*19*) for the 1° grid at 18°S, 146°E (resampled to 5-year averages, 1905 to 1985). Linear regressions are signif-

[1]Research School of Earth Sciences, Australian National University, Canberra, ACT 0200, Australia. [2]Australian Institute of Marine Science, PMB 3, Townsville M.C., Queensland 4810, Australia.

*To whom correspondence should be addressed. E-mail: erica.hendy@anu.edu.au